

## Article

# Calculation of Shear Layer Thickness of Ionic Rare Earth Particles in Mixture Electrolytes during In-Situ Leaching Process

Zhongquan Gao<sup>1</sup>, Yunzhang Rao<sup>1,\*</sup>, Xiaoming Zhang<sup>2</sup>, Wei Xu<sup>1</sup>, Zhihua Yang<sup>1</sup> and Run Xiang<sup>1</sup>

<sup>1</sup> School of Resources and Environmental Engineering, Jiangxi University of Science and Technology, Ganzhou 341000, China

<sup>2</sup> School of Civil and Surveying & Mapping Engineering, Jiangxi University of Science and Technology, Ganzhou 341000, China

\* Correspondence: raoyunzhang@jxust.edu.cn; Tel.: +86-150-8378-1770

**Abstract:** During in-situ mining and leaching of ionic rare earth ore, a chemical replacement reaction occurs between the leaching agent and rare earth ore. The thickness of the shear layer on the surface of colloidal particles is an important physical parameter. Based on the Gouy–Chapman double-layer theory and Poisson–Boltzmann equation, the relational expression for the thickness of the shear layer in the electric double layer on the particle surface under the condition of 2:2 + 3:2 mixture electrolytes ( $\text{MgSO}_4 + \text{RE}_2(\text{SO}_4)_3$ ) is derived. On this basis, an indoor column leaching experiment of  $\text{MgSO}_4$  solution is conducted, and the surface Zeta potential of rare earth ore particles is measured using a Zetaprobe potential analyzer. The surface potential and the thickness of the shear layer in the leaching process with different concentrations solutions (2.5%, 3.0%, and 3.5%) are calculated. The effects of a  $\text{MgSO}_4$  solution concentration and particle surface potential on the thickness of the shear layer in the electric double layer are analyzed. It provides a theoretical basis for the study of the internal seepage of the ore body under the condition of the coexistence of multiple ions in the leaching process.

**Keywords:** ionic rare earth; diffuse double layer; Zeta potential; Poisson–Boltzmann equation



**Citation:** Gao, Z.; Rao, Y.; Zhang, X.; Xu, W.; Yang, Z.; Xiang, R.

Calculation of Shear Layer Thickness of Ionic Rare Earth Particles in Mixture Electrolytes during In-Situ Leaching Process. *Minerals* **2023**, *13*, 733. <https://doi.org/10.3390/min13060733>

Academic Editors: Chiharu Tokoro and Przemyslaw B. Kowalczyk

Received: 30 March 2023

Revised: 22 May 2023

Accepted: 26 May 2023

Published: 29 May 2023



**Copyright:** © 2023 by the authors. Licensee MDPI, Basel, Switzerland. This article is an open access article distributed under the terms and conditions of the Creative Commons Attribution (CC BY) license (<https://creativecommons.org/licenses/by/4.0/>).

## 1. Introduction

Ionic rare earth is an indispensable strategic resource in the field of high-tech industry and national defense [1]. It mainly exists on the surface of minerals in the form of ions, such as halloysite, illite, kaolinite, and a small amount of montmorillonite in the deposit. The only way to extract rare earth elements is to use a salt electrolyte solution to leach ion-adsorbed rare earth deposits [2–5]. Flotation is usually used to pre-treat ores containing valuable metals before leaching [6–8]. In the process of leaching, the negative charges on the surface of the particles, the cations subjected to electrostatic attraction, and the polar water molecules together form the diffuse double-layer structure of the clay particles [9,10]. The thickness of the shear layer is a significant parameter, referring to the distance between the shear plane and the surface of particles, which is closely related to the properties of the colloids, such as electroosmosis, electrophoresis, and flow potential [11,12]. It depends largely on the type of clay, the concentration, and the valence of ions in pore water [13].

The models for studying the diffuse double-layer theory include the Helmholtz double-layer model, the Debye–Hückel approximation, and the Gouy–Chapman theory. The most famous one, the Gouy–Chapman theory, applied the Poisson–Boltzmann equation to the diffuse double layer and obtained its analytical solution in 1910–1913 [14]. Related research works [15,16] used  $1/k$  to calculate the thickness of the double layer and analyzed the effects of various factors, including concentration and particle shape, on it. Chang et al. [17] obtained the influence of electrolyte type and surface charge density on the diffuse layer by solving the Poisson–Boltzmann equation that considers parameters such as ion radius and

electrolyte concentration. Nishiya-ma et al. [18] studied the effects of ionic strength, pH, and mineral type on the water film thickness in porous media by numerically solving the Poisson–Boltzmann equation based on the effect of a three-layer model and double-layer overlap. Shakila and Pandou et al. [19,20] studied that the thickness of the shear layer is 0.03  $\mu\text{m}$ , 0.1  $\mu\text{m}$ , less than 0.25  $\mu\text{m}$ , and no more than 2  $\mu\text{m}$ . They regarded the particle surface potential value as infinite. Wang et al. [21] found that the thickness of the shear layer varied from 2.10 to 2.7 nm by leaching with different concentrations of  $(\text{NH}_4)_2\text{SO}_4$  solution. At high electrolyte concentrations, the ion volume effect and dispersion force become very important [22,23]. However, the Poisson–Boltzmann equation is still accurate under low electrolyte concentration conditions [24]. The above analysis shows that the thickness of the shear layer obtained by different researchers is very different, mainly because the surface potential value of the colloidal particles is difficult to accurately determine.

Therefore, in this paper, based on the Poisson–Boltzmann equation, a formula for calculating the thickness of the shear layer in the electric double layer on the particle surface under the condition of 2:2 + 3:2 mixture electrolytes ( $\text{MgSO}_4 + \text{RE}_2(\text{SO}_4)_3$ ) is derived by using indoor simulated column leaching methods and using a  $\text{MgSO}_4$  solution with different concentrations (2.5%, 3.0%, and 3.5%) as leaching agent. Meanwhile, the effect of the  $\text{MgSO}_4$  solution concentration and particle surface potential on the thickness of the shear layer in the electric double layer of the particle surface is analyzed. This analysis provides support for further enriching and perfecting the theory of colloidal diffuse double-layer structure and provides a theoretical basis for the study of the internal seepage of the ore body under the condition of the coexistence of multiple ions in the leaching process.

## 2. Construction of Theoretical Model

For electrolyte solutions with any valence, the nonlinear Poisson–Boltzmann equation is [21,25]:

$$\frac{dy}{dx} = \sqrt{\frac{8\pi F^2}{\varepsilon RT} \sum_i c_i [\exp^{-Z_i y} - 1]} \quad (1)$$

where  $F$  is the Faraday constant ( $F = 96,490 \text{ C/mol}$ );  $\varepsilon$  is the dielectric constant of the medium, unit  $\text{C}^2/(\text{J}\cdot\text{m})$ ;  $R$  is the gas constant ( $R = 8.314 \text{ J/mol}\cdot\text{K}$ );  $T$  is the absolute temperature (K);  $c_i$  is the ion concentration, unit mol/L; and  $Z_i$  is the valence of ions.

When using a  $\text{MgSO}_4$  solution as a leaching agent, ion exchange occurs between the  $\text{Mg}^{2+}$  in the solution and the  $\text{RE}^{3+}$  in the ore sample. At this time, the electrolyte in the pore solution is a 2:2 + 3:2 mixture electrolyte ( $\text{MgSO}_4 + \text{RE}_2(\text{SO}_4)_3$ ,  $\text{CD} + \text{E}_2\text{F}_3$ ), and Equation (1) can be converted to

$$\frac{dy}{dx} = \sqrt{\frac{8\pi F^2}{\varepsilon RT} [c_C (e^{-Z_C y} - 1) + c_D (e^{-Z_D y} - 1) + c_E (e^{-Z_E y} - 1) + c_F (e^{-Z_F y} - 1)]} \quad (2)$$

where  $c_C$ ,  $c_D$ ,  $c_E$ , and  $c_F$  are the concentrations of magnesium ion, sulfate ion corresponding to magnesium ion, rare earth ion, and sulfate ion corresponding to rare earth ion, respectively, unit mol/L;  $Z_C$ ,  $Z_D$ ,  $Z_E$ , and  $Z_F$  are the valences of magnesium ions, sulfate ions corresponding to magnesium ions, rare earth ions, and sulfate ions corresponding to rare earth ions, respectively.

For  $\text{MgSO}_4$ ,  $c_C = c_D$ ,  $Z_C = 2$ ,  $Z_D = -2$ ;

For  $\text{RE}_2(\text{SO}_4)_3$ ,  $1.5c_E = c_F$ ,  $Z_E = 3$ ,  $Z_F = -2$ ;

Equation (2) can be transformed into

$$\frac{dy}{dx} = \sqrt{\frac{8\pi F^2}{\varepsilon RT} [c_C (e^{-2y} - 1) + c_C (e^{2y} - 1) + c_E (e^{-3y} - 1) + 1.5c_E (e^{2y} - 1)]} \quad (3)$$

Introducing  $y(x) = \frac{F\psi(x)}{RT}$  into Equation (3), the potential distribution function  $\psi(x)$  can be expressed as

$$\psi(x) = \frac{RT}{F} \ln \left( 1 - \frac{2(4c_C + 4.5c_E)\lambda_1 e^{\kappa_1 x}}{(\lambda_1 e^{\kappa_1 x} + 2c_C + 3c_E)^2 - (c_C + 1.5c_E)(4c_C + 4.5c_E)} \right) \quad (4)$$

where  $\lambda_1, \kappa_1$  are constants; the expressions of  $\lambda_1, \kappa_1$  are shown in Equations (5) and (6):

$$\lambda_1 = \frac{(4c_C + 4.5c_E)}{1 - e^{\frac{F\psi_0}{RT}}} - (2c_C + 3c_E) + \sqrt{(4c_C + 4.5c_E) \left[ (c_C + 1.5c_E) - \frac{(4c_C + 6c_E)}{1 - e^{\frac{F\psi_0}{RT}}} + \frac{(4c_C + 4.5c_E)}{\left(1 - e^{\frac{F\psi_0}{RT}}\right)^2} \right]} \quad (5)$$

$$\kappa_1 = \sqrt{\frac{8\pi F^2(4c_C + 4.5c_E)}{\epsilon RT}} \quad (6)$$

where  $\psi_0$  is the surface potential, unit V.

By substituting the potential value  $\zeta$  for  $\psi(x)$ , the thickness of the shear layer  $x_s$  can be obtained with

$$x_s = \frac{1}{\kappa_1} \ln \frac{\left( (4c_C + 4.5c_E) - (2c_C + 3c_E) \left(1 - e^{\frac{F\zeta}{RT}}\right) + \sqrt{(4c_C + 4.5c_E) \left[ (c_C + 1.5c_E) \left(1 - e^{\frac{F\zeta}{RT}}\right)^2 - (4c_C + 6c_E) \left(1 - e^{\frac{F\zeta}{RT}}\right) + (4c_C + 4.5c_E) \right]} \right)}{\lambda_1 \left(1 - e^{\frac{F\zeta}{RT}}\right)} \quad (7)$$

where  $\zeta$  is Zeta potential, unit V.

When the initial concentration of the  $\text{MgSO}_4$  solution in the pores of the ore body is extremely low, or the influence of the rare earth ions on the bulk solution can be ignored after the leaching is completed, the solution around the ore particles is a single 2:2 electrolyte ( $\text{MgSO}_4$ , AB). The thickness of the shear layer  $x_s$  in a single electrolyte is expressed as [26]

$$x_s = \frac{1}{\kappa_2} \ln \left[ \frac{8 + 8e^{\frac{\zeta F}{RT}}}{\lambda_2 \left(1 - e^{\frac{\zeta F}{RT}}\right)} \right] \quad (8)$$

The expressions of  $\lambda_2$  and  $\kappa_2$  are as follows:

$$\lambda_2 = \frac{8 + 8e^{F\psi_0/RT}}{\lambda \left(1 - e^{\frac{F\psi_0}{RT}}\right)} \quad (9)$$

$$\kappa_2 = \sqrt{\frac{32\pi F^2 Z_A^2 c_A}{\epsilon RT}} \quad (10)$$

### 3. Materials and Methods

The samples of rare earth, taken from Zudong rare earth deposits in Longnan County, Jiangxi province, were designed as a cylinder with a diameter of 44 mm and a height of 60 mm. The chemical element composition of the original rare earth was analyzed using an X-ray fluorescence spectrometer (XRF, Axios max type produced by PANalytical B. V., Almelo, The Netherlands). The chemical element content of each component was obtained, as shown in Table 1. Three groups of  $\text{MgSO}_4$  solution with different concentrations (2.5%, 3.0%, and 3.5%) were prepared for leaching with the method of simulated column leaching. The experimental process is shown in Figure 1.

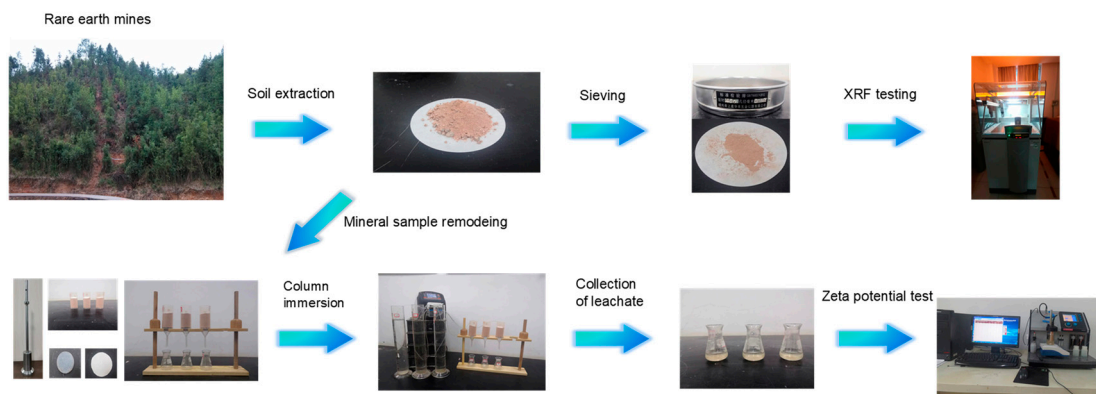


**Figure 1.** Experimental flow chart.

- (1) EDTA volumetric titration analysis. EDTA titration test solution was configured to test the leaching solution of rare earth collected every hour. An amount of 5 mL of rare earth leaching solution was added to the acid burette and titrated with EDTA solution until the test solution in the burette turned bright yellow. The amount of EDTA test solution was recorded.
- (2) Zeta potential test. Three groups of  $\text{MgSO}_4$  solution with different concentrations (2.5%, 3.0%, and 3.5%) were prepared for column leaching. The leaching solutions were collected every hour, and the Zeta potentials were tested at room temperature using a Zeta potential analyzer produced by Colloidal Dynamics, Ponte Vedra Beach, FL, USA.

**Table 1.** Chemical element content Unit: %.

Compound Formula	O	Na	Mg	Al	Si	S	Cl	K	Ca	Ti	Mn	
Concentration	55.251	0.112	0.079	18.761	21.733	0.011	0.006	1.408	0.064	0.020	0.056	
Compound formula	Fe	Ni	Zn	Ga	Rb	Y	Zr	Nd	Yb	W	Pb	Th
Concentration	1.263	0.003	0.014	0.006	0.034	0.068	0.019	0.024	0.011	0.005	0.034	0.006

## 4. Results and Discussion

### 4.1. Rare Earth Ion Leaching Analysis

It can be seen from Figure 2 that with the increase in the  $\text{MgSO}_4$  solution concentration, the concentration of rare earth ions and the leaching rate of rare earth increase, and the leaching rate of the leaching solution decreases gradually. Figure 2a shows that in the first period of leaching, there is almost no leaching of rare earth ions and that the leaching solution does not fully penetrate the soil column. At this time, the soil sample is in the saturated stage. With the increase of time, the  $\text{MgSO}_4$  solution begins to replace the rare earth elements in the ore sample; thus, more rare earth elements can be detected in the leaching solution. After the leaching process enters the third hour, it is found that a large amount of rare earth is precipitated at this stage, and the concentration of rare earth ions reaches a peak at this time. At the fourth to sixth hours, it can be seen that the rare earth leaching rate slows down. In the subsequent stage, the concentration of rare earth ions gradually decreases. After the 7th hour, the rare earth content in the leaching solution is gradually reduced. By the 8th hour, rare earth ions are almost undetectable, and it is determined that the reaction is completed at this time. The whole process of magnesium sulfate leaching can be divided into four stages [27]: preparation stage (0–1 h), initial reaction stage (2–3 h), main reaction stage (4–6 h), and tailing stage (7–8 h). In Figure 2b, we see that the rare earth leaching rate reaches its highest (79.84%) when the 3.5%  $\text{MgSO}_4$  solution is used for leaching. The leaching rate of the three groups leached with different concentrations of  $\text{MgSO}_4$  solutions is almost 0 in 0–1 h. After 1 h of leaching, the leaching rate begins to rise rapidly, reaching the maximum around 6–7 h, and finally tends to be

stable. From Figure 2c, it can be seen that during the leaching process of three groups of  $\text{MgSO}_4$  solutions with different concentrations, the leaching rate of the solution increases first and then decreases greatly, and finally tends to be stable. Since the  $\text{MgSO}_4$  solution belongs to the electrolyte solution, when the solid soil particles come into contact with the  $\text{MgSO}_4$  solution, the charged ions on the surface of the soil particles rearrange to form an electric double layer, and the double layer on the surface of the fine particles has an electroviscous effect [28,29]. When the solution flows under the action of hydraulic gradient, the net charge in the electric double layer also flows with the solution, and the potential difference is formed at both ends of the microscopic pore channel, that is, the streaming potential. The negative gradient is called the flow-induced electric field [30]. The net charge flowing with the solution flows backward under the action of the flow-induced electric field, and the viscous force of the net charge drives the solution to flow backward together, resulting in a decrease in the leaching rate of the  $\text{MgSO}_4$  solution. Finally, the solution is subjected to the van der Waals force on the fine particle surface, causing the solution to produce additional cohesion and the leaching rate of the solution to decrease [31].

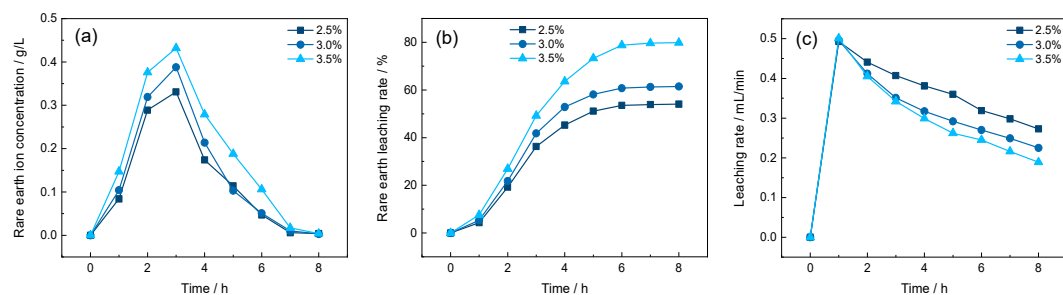


**Figure 2.** (a) Concentration of rare earth ion; (b) Rare earth leaching rate; (c) Leaching rate.

#### 4.2. Comparative Analysis of Zeta Potential and Surface Potential Values

There is a large number of negatively charged chemical bonds on the surface of clay minerals. The breaking crystal plane causes the exposure of the Si–O tetrahedral layer and the Al–O octahedral layer. The  $\text{Si}^{4+}$  on the surface is replaced by the isomorphous  $\text{Al}^{3+}$  to form a certain amount of permanent negative charges, which are adsorbed on the surface of clay minerals to maintain a stable state of neutral electricity [32–34]. According to references [21,25], the surface potential of 2:2 + 3:2 mixture electrolyte at different concentrations was calculated, which was different from Chariton et al. [35,36], who approximated the Zeta potential as the surface potential.

The average ion concentration of mixture electrolytes is [21,25,37]

$$c(x) = c_C \exp\left(-z_C \frac{F\psi(x)}{RT}\right) + c_E \exp\left(-z_E \frac{F\psi(x)}{RT}\right) \quad (11)$$

where  $c(x)$  is the concentration of adsorbed ions from the surface of the solid particles to the  $x$  distance, unit mol/L.

The average ion concentration  $c_1$  is

$$c_1 = \kappa \int_0^{1/\kappa} c(x) dx \quad (12)$$

The surface potential can be obtained by solving the following equation by numerical method:

$$\kappa \int_0^{1/\kappa} c(x) dx = \frac{CEC \cdot \kappa}{S} \quad (13)$$

where  $CEC$  represents cation exchange capacity, unit mol/kg;  $S$  is the specific surface area of the particles,  $\text{m}^2/\text{g}$ ;  $1/\kappa$  is the thickness of the double layer.

The expressions of  $\psi(x)$ ,  $\lambda_1$ , and  $\kappa_1$  in the above equation have been obtained in Section 2. This equation is a nonlinear equation with  $\psi_0$  as unknown. The surface potential

$\psi_0$  can be obtained by solving the nonlinear equation with the fixed-point method. It can be seen from the equation of the electric double layer theory that the factors affecting the soil/liquid interface potential of the colloid include the charge density of the particles, the electrolyte concentration, the ion valence, etc.

As shown in Figure 3, when using different concentrations of the  $\text{MgSO}_4$  solution for leaching, with the increase in leaching time, the absolute value of Zeta potential on the surface of rare earth mineral particles gradually decreases, and the absolute value of surface potential gradually increases. When using 2.5%, 3.0%, and 3.5%  $\text{MgSO}_4$  solutions, the maximum difference between Zeta potential and surface potential was 12.49 mv, 7.94 mv, and 19.10 mv, respectively. This also indicated that the position of the shear plane was close to the outer edge of the diffuse layer, and the shear layer was far from the Stern distance of the particle surface. The surface potential of the colloidal particles is different from the Zeta potential value. Thus, it is feasible to calculate the shear layer thickness according to the surface potential and Zeta potential of different particles. When the concentration of the  $\text{MgSO}_4$  solution was 3.5%, Zeta potential had the largest magnitude of change with a variation of 21.4 mv. When the concentration was 2.5%, the Zeta potential had the largest variation, reducing by 44.72%. The variation of surface potential was also the largest, increasing by 49.77%. Due to the strong hydrophobicity of the surface of rare earth minerals, more  $\text{Mg}^{2+}$  entered the particle surface, and the ionized impurity ions were adsorbed onto the particle surface to compress the double layer, resulting in a decrease in the absolute value of Zeta potential [5,38,39].

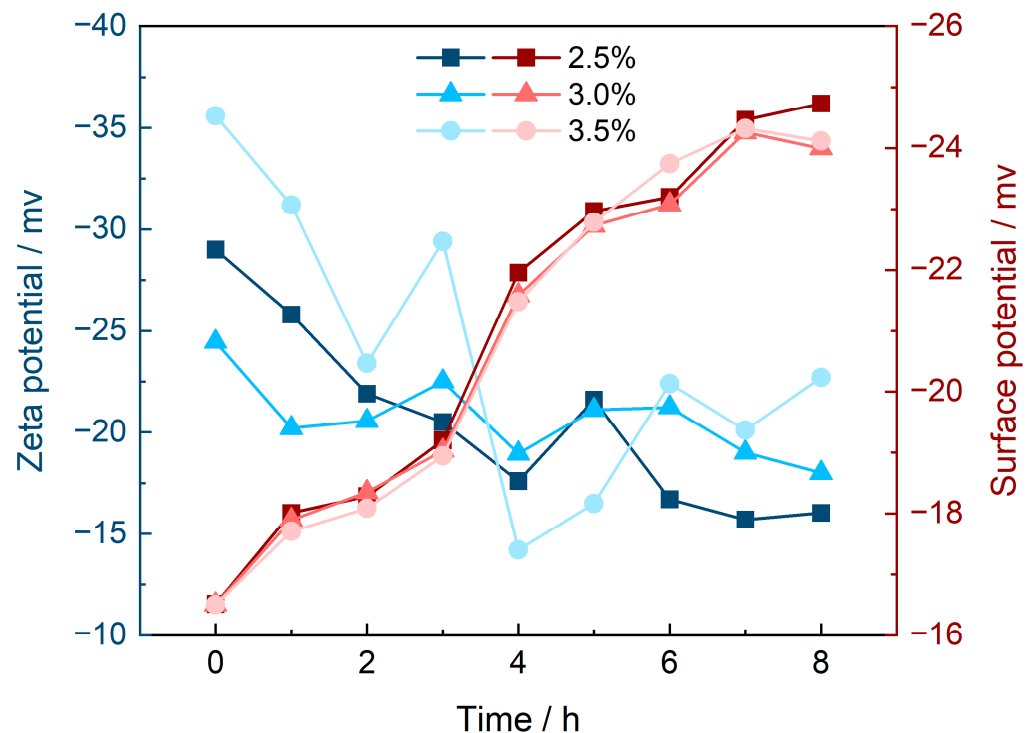


**Figure 3.** Potential variation diagram.

#### 4.3. Analysis of the Shear Layer Thickness

On the surface of the soil, the colloid has a large amount of charge. When the soil colloid contacts with the aqueous solution, the surface of the soil colloid adsorbs the counter-charged ions from the solution. Due to the electrostatic attraction, a double-layer structure is ultimately formed [39,40]. According to the potential distribution expression in the double layer theory [41,42], the thickness of the shear layer can be calculated by substituting the data of the surface potential and Zeta potential in Section 4.2 into Equation (7).

Figure 4 shows the variation curves of the thickness of the shear layer and the thickness of the double layer ( $1/\kappa$ ) during the leaching process of solutions with different concentra-

tions. The thickness of the shear layer changed gently and showed a decreasing trend. The thickness of the electric double layer decreased first, then increased rapidly, then decreased sharply, and finally decreased slowly. With the increase in concentration, the thickness of the double layer decreased gradually and reached the maximum at 3 h. The thickness of the shear layer was less than that of the electric double layer. The shear layer was far from the Stern layer in the electric double layer, that is, near the Gouy layer. When the  $\text{MgSO}_4$  solution with a concentration of 3.5% was used for leaching, the change in the thickness of the shear layer was the largest, from 14.34 nm to 1.18 nm, which was reduced by 91.80%. The ions contained in the electric double layer were constantly changing, as well as the surface potential value and Zeta potential of colloidal particles, which jointly determined the thickness of the shear layer. Therefore, the greater the difference in the variation trend between them, the greater the difference in the obtained thickness value of the shear layer. When  $\text{MgSO}_4$  solutions with different concentrations were used for leaching, the difference in the thickness of the shear layer was 11.16 nm, 6.61 nm, and 13.16 nm, respectively. This was consistent with the results of Yang et al. [11], that the average thickness of the shear layer on the particle surface varied between 3.0–3.3 nm. The  $\text{Mg}^{2+}$  in the leaching agent reacted with the  $\text{RE}^{3+}$  in the rare earth ore faster. Under the strong exchange reaction, the interaction force between the particles played a key role in the aggregation/dispersion process of the soil particles. If the net force was shown as gravitational force, the aggregation process occurred. If the net force was shown as a repulsive force, the dispersion process occurred. The thickness of the shear layer was affected accordingly. In the results of aggregation/dispersion of soil colloidal particles or clay particles, the electric double layer of clay particles was greatly affected, and the thickness of the shear layer presented a decreasing trend. At this time, van der Waals gravity played a leading role, making the clay particles closer together [43]. Through the aggregation/dispersion process of soil particles, the stability of soil structure was affected, the distribution of pore size in soil was changed, and finally, the seepage effect of the leaching agent was affected.

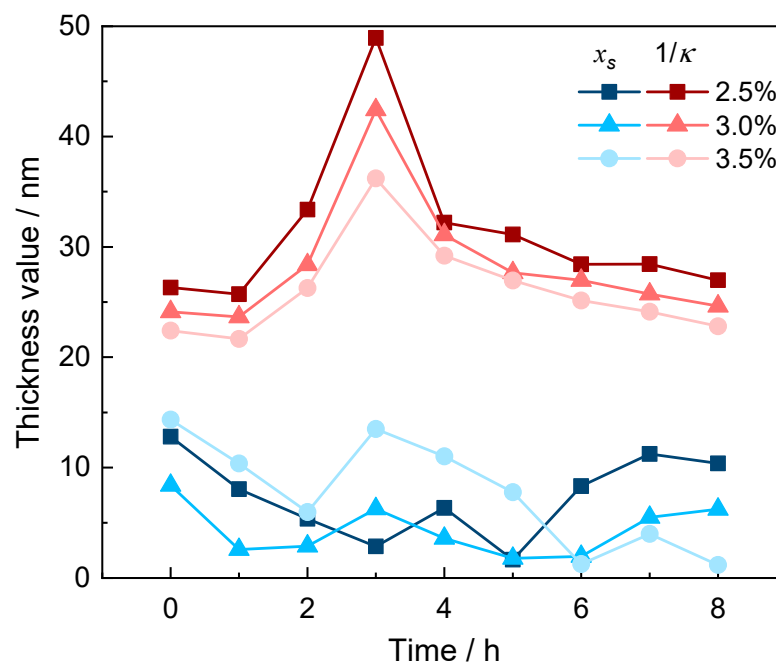


Figure 4. Variation curve of  $x_s$  and  $1/\kappa$  in the leaching process.

## 5. Conclusions

In this paper, based on the Gouy–Chapman double layer theory and Poisson–Boltzmann equation, the expression for calculating the thickness of the shear layer in the electric double layer of the particle surface under the condition of 2:2 + 3:2 mixture electrolytes ( $\text{MgSO}_4 + \text{RE}_2(\text{SO}_4)_3$ ) is derived. Three groups of  $\text{MgSO}_4$  solution with different mass

concentrations of 2.5%, 3.0%, and 3.5% are used for the indoor column leaching test. The overall performance shows that the leaching rate of the solution increases first and then decreases significantly, and finally stabilizes. The maximum difference between Zeta potential and surface potential is 12.49 mV, 7.94 mV, and 19.10 mV, respectively. The shear layer is far from the Stern layer in the electric double layer, and its thickness is less than the thickness of the double layer. With the increase of  $\text{MgSO}_4$  solution concentration, the concentration of rare earth ions and the leaching rate of rare earth increases while the leaching rate of leaching solution decreases gradually. The thickness of the electric double layer decreases gradually and reaches the maximum at 3 h. When the 3.5%  $\text{MgSO}_4$  solution is used for leaching, the Zeta potential has the largest change with the variation of 21.4 mv. The leaching rate of rare earth is the highest (79.84%), and the thickness of the shear layer has the largest variation, with a reduction of 91.80% from 14.34 nm to 1.18 nm. The  $\text{Mg}^{2+}$  in the leaching agent reacts more quickly with the  $\text{RE}^{3+}$  in the rare earth ore. Under the strong exchange reaction, the electric double layer of the clay particles is compressed, and the thickness decreases. At this time, van der Waals gravity plays a major role, making the clay particles closer together.

**Author Contributions:** Conceptualization, Z.G. and Y.R.; methodology, Z.G.; software, Z.G., R.X. and X.Z.; validation, W.X.; data curation, Z.G.; writing—original draft preparation, Z.G. and Y.R.; writing—review and editing, Z.G., Y.R. and X.Z.; visualization, W.X., R.X., X.Z. and Z.Y.; supervision, Y.R.; project administration, Y.R.; funding acquisition, Y.R. All authors have read and agreed to the published version of the manuscript.

**Funding:** This research was supported by the National Natural Science Foundation of China (51964014).

**Data Availability Statement:** Not applicable.

**Acknowledgments:** Thanks for the great effort by editors and reviewers.

**Conflicts of Interest:** The authors declare no conflict of interest.

## References

1. Dong, Y.F.; Feng, M.; Liu, Z.X.; Wu, Y.F.; Li, Y.L.; Wu, W.Y. Numerical simulation of double electric layer-thermal field coupling in bottom cathode rare earth electrolytic cell. *Chin. Rare Earths* **2019**, *40*, 88–94.
2. Wang, X.J.; Wang, H.; Sui, C.; Zhou, L.B.; Feng, X.; Huang, C.G.; Zhao, K.; Zhong, W.; Hu, K.J. Permeability and adsorption-desorption behavior of rare earth in laboratory leaching tests. *Minerals* **2020**, *10*, 889. [\[CrossRef\]](#)
3. Moldoveanu, G.A.; Papangelakis, V.G. Recovery of rare earth elements adsorbed on clay minerals: I. Desorption mechanism. *Hydrometallurgy* **2012**, *117*, 71–78. [\[CrossRef\]](#)
4. Wang, D.; Wu, F.W.; Rao, Y.Z.; Xu, W.; Han, M.; Shi, L. Simulation of an ionic rare earth leaching process based on the darcy law-chemical reaction engineering-transfer of dilute substance coupling. *Minerals* **2022**, *12*, 1500. [\[CrossRef\]](#)
5. Gao, Z.Q.; Rao, Y.Z.; Shi, L.; Xiang, R.; Yang, Z.H. Effect of magnesium sulfate solution on pore structure of ionic rare earth ore during leaching process. *Minerals* **2023**, *13*, 294. [\[CrossRef\]](#)
6. Zhao, W.J.; Wang, M.L.; Yang, B.; Feng, Q.C.; Liu, D.W. Enhanced sulfidization flotation mechanism of smithsonite in the synergistic activation system of copper-ammonium species. *Miner. Eng.* **2022**, *187*, 107796. [\[CrossRef\]](#)
7. Feng, Q.C.; Yang, W.H.; Wen, S.M.; Wang, H.; Zhao, W.J.; Han, G. Flotation of copper oxide minerals: A review. *Int. J. Min. Sci. Technol.* **2022**, *32*, 1351–1364. [\[CrossRef\]](#)
8. Zhou, H.P.; Yang, Z.Z.; Zhang, Y.B.; Han, H.S.; He, K.Z.; Luo, X.P. Enhanced flotation of hemimorphite: Adjusting mineral surface potential with sodium thiocyanate as activator. *Miner. Eng.* **2021**, *171*, 107088. [\[CrossRef\]](#)
9. Helmholtz, H. Ueber einige gesetze der vertheilung elektrischer ströme in körperlichen leitern, mit anwendung auf die thierisch-elektrischen versuche. *Ann. Phys.* **1853**, *165*, 353–377. [\[CrossRef\]](#)
10. Van, O. *Introduction to Clay Colloid Chemistry*; Agricultural Press: Beijing, China, 1982.
11. Yang, T.S.; Xiong, X.Z.; Zhan, X.L.; Yang, M.Q. The Study on slipping water layers of cohesive sediment particles. *Shuili Xuebao* **2002**, *5*, 20–25.
12. Ding, W.Q.; Zhu, Q.H.; Wang, L.; Luo, Y.X.; Li, Q.; Zhu, H.L.; Hu, F.N.; Zhu, L.H.; Li, H. Calculation of thickness of shear plane in diffuse double layer of constant charge soil colloid in single electrolyte system. *Acta Pedol. Sin.* **2015**, *52*, 859–868.
13. Mahanta, K.K.; Mahanta, G.C.; Mishra, M.L. Estimation of electric double layer thickness from linearized and nonlinear solutions of Poisson-Boltzman equation for single type of ions. *Appl. Clay Sci.* **2012**, *59*, 1–7. [\[CrossRef\]](#)
14. Zhang, Q.; Li, F.H.; Li, F.C.; Guo, Z.Y.; Chu, Z.; Pai, K.H. Research progress of the theory of electric double layer on electrode/ionic liquids for supercapacitors. *Guangdong Chem. Ind.* **2021**, *48*, 120–122.

15. Gu, P.; Yang, S.; Liu, X.T.; Yang, G. Development of a simple, molecular dynamics-based method to estimate the thickness of electrical double layers. *Soil. Sci. Soc. Am. J.* **2020**, *84*, 494–501. [[CrossRef](#)]
16. Shang, F.; Yang, C.S.; Zhang, L.H.; Zhou, C.L.; Han, D.W.; Shi, Y.J. Analysis of influencing factors of clay particle diffusion in electric double layer. *J. Glaciol. Geocryol.* **2022**, *44*, 495–505.
17. Chang, F.; Sposito, G. The electrical double layer of a disk-shaped clay mineral particle: Effect of particle size. *J. Colloid Interface Sci.* **1994**, *163*, 19–27. [[CrossRef](#)]
18. Nishiyama, N.; Yokoyama, T. Water film thickness in unsaturated porous media: Effect of pore size, pore solution chemistry, and mineral type. *Water Resour. Res.* **2021**, *57*, e2020WR029257. [[CrossRef](#)]
19. Shakila, B. Surface potential and shear plane thickness for a treated concrete particulate. *J. Colloid. Interface Sci.* **2003**, *261*, 399–401.
20. M'pandou, A.; Siffert, B. Polyethyleneglycol adsorption at the TiO<sub>2</sub> H<sub>2</sub>O interface: Distortion of ionic structure and shear plane position. *Colloids Surf.* **1987**, *24*, 159–172. [[CrossRef](#)]
21. Wang, J.; Wang, G.S.; Hong, B.G. Effects of concentration of pore solution on stability of ion-absorbed rare earth ore aggregate. *Adv. Civ. Eng.* **2021**, *2021*, 8846605. [[CrossRef](#)]
22. Aniban, X.; Hartwig, B.; Wuttke, A.; Mata, R.A. Dispersion forces in chirality recognition—a density functional and wave function theory study of diols. *Phys. Chem. Chem. Phys.* **2021**, *23*, 12093–12104. [[CrossRef](#)] [[PubMed](#)]
23. Chen, Z.Y.; Sun, L.J.; Liu, C.Y.; Wang, C.; Xu, B.C. The ion specific effect on the aggregation behaviors of surfactants. *China Clean. Ind.* **2022**, *8*, 60–69.
24. Fu, S.; Yu, Y.X.; Wang, X.L. Theoretical investigation on the separation characteristics of electrolyte solutions with the nanofiltration membranes (II): Mixed electrolyte solutions. *Acta Chim. Sin.* **2007**, *10*, 923–929.
25. Liu, X.M.; Li, H.; Li, R.; Tian, R. Analytical solutions of the nonlinear Poisson–Boltzmann equation in mixture of electrolytes. *Surf. Sci.* **2013**, *607*, 197–202. [[CrossRef](#)]
26. Ding, W.Q.; Liu, X.M.; Song, L.; Li, Q.; Zhu, Q.H.; Zhu, H.L.; Hu, F.N.; Luo, Y.X.; Zhu, L.H.; Li, H. An approach to estimate the position of the shear plane for colloidal particles in an electrophoresis experiment. *Surf. Sci.* **2015**, *632*, 50–59. [[CrossRef](#)]
27. Tan, S.J.; Rao, Y.Z.; Zhang, M.D.; Wang, D.; Zhang, S.J.; Wu, F.Y. Study on seepage evolution law of ionic rare earth ore leached by magnesium sulfate. *Nonferrous Met. Sci. Eng.* **2023**, 1–10.
28. Torkzaban, S.; Bradford, S.A.; Vanderzalm, J.L.; Patterson, B.M.; Harris, B.; Prommer, H. Colloid release and clogging in porous media: Effects of solution ionic strength and flow velocity. *J. Contam. Hydrol.* **2015**, *181*, 161–171. [[CrossRef](#)]
29. Deng, Q.J.; Zhu, W.Y.; Wang, X.F.; Sui, X.G.; Wang, X.J. Seepage model considering micro forces in porous media. *Chin. J. Eng.* **2014**, *36*, 415–423.
30. Thanh, L.D.; Jougno, D.; Phan, V.D.; Nguyen, X.C.; Nguyen, T.H. A physically based model for the streaming potential coupling coefficient in partially saturated porous media. *Water* **2020**, *12*, 1588. [[CrossRef](#)]
31. Zhang, X.M.; Gao, Z.Q.; Rao, Y.Z.; Shi, L.; Xu, W. Evolutionary law of pore structure of ion-adsorbed rare earth ore leaching process. *Minerals* **2023**, *13*, 322. [[CrossRef](#)]
32. Aksoy, Y.Y.; Kaya, A. A study of factors affecting on the zeta potential of kaolinite and quartz powder. *Environ. Earth Sci.* **2011**, *62*, 697–705. [[CrossRef](#)]
33. Li, H.L.; Min, F.F.; Peng, C.L. Zeta potential simulation of Kaolinite particle surface in different Ca<sup>2+</sup> concentration and pH value suspension. *J. China Univ. Min. Technol.* **2013**, *42*, 631–637.
34. Hu, Y.X. Surface zeta potential and surface absorption—a theoretical explanation of the rule of coagulation. *Chin. J. Struct. Chem.* **1992**, *11*, 447.
35. Charlton, I.D.; Doherty, A.P. Locating the micellar shear plane and its relationship with the Debye screening length. *J. Phys. Chem. B* **1999**, *103*, 5081–5083. [[CrossRef](#)]
36. Adamson, A.W.; Klerer, J. Physical chemistry of surfaces. *J. Electrochem. Soc.* **1977**, *124*, 192C. [[CrossRef](#)]
37. Li, H.; Qing, C.L.; Wei, S.Q.; Jiang, X.J. An approach to the method for determination of surface potential on solid/liquid interface: Theory. *J. Colloid. Interface Sci.* **2004**, *275*, 172–176. [[CrossRef](#)]
38. Li, H.P.; Hu, Y.H.; Wang, D.Z.; Xu, J. Mechanism of interaction between cationic surfactant and kaolinite. *J. Cent. South Univ. (Sci. Technol.)* **2004**, *2*, 228–233.
39. Zhang, Z.J.; Liu, J.T.; Feng, L.; Zhou, W.J. A prediction model based on Langmuir theory for equilibrium adsorption amount. *J. Northeast. Univ. (Nat. Sci.)* **2011**, *32*, 749–751+756.
40. Yang, K.L.; Yiacoymi, S.; Tsouris, C. Monte Carlo simulations of electrical double-layer formation in nanopores. *J. Chem. Phys.* **2002**, *117*, 8499–8507. [[CrossRef](#)]
41. Zhao, X.C. Influences of Stern potential and electric concentration on foam stability. *Chem. Eng. Des. Commun.* **2019**, *45*, 190–192.
42. Li, H.; Hou, J.; Liu, X.M.; Li, R.; Zhu, H.L.; Wu, L.S. Combined determination of specific surface area and surface charge properties of charged particles from a single experiment. *Soil Sci. Soc. Am. J.* **2011**, *75*, 2128–2135. [[CrossRef](#)]
43. Zhu, H.L.; Li, B.; Xiong, H.L.; Li, H.; Jia, M.Y. Dynamic light scattering study on the aggregation kinetics of soil colloidal particles in different electrolyte systems. *Acta Phys. Chim. Sin.* **2009**, *25*, 1225–1231.

**Disclaimer/Publisher's Note:** The statements, opinions and data contained in all publications are solely those of the individual author(s) and contributor(s) and not of MDPI and/or the editor(s). MDPI and/or the editor(s) disclaim responsibility for any injury to people or property resulting from any ideas, methods, instructions or products referred to in the content.